Magnetic structure of the spin-1/2 frustrated quasi-one-dimensional antiferromagnet $Cu_3Mo_2O_9$: Appearance of a partial disordered state

Masashi Hase[1],* Haruhiko Kuroe[2], Vladimir Yu. Pomjakushin[3], Lukas Keller[3], Ryo Tamura[1], Noriki Terada[1], Yoshitaka Matsushita[1], Andreas Dönni[1], and Tomoyuki Sekine[2]
[1]*National Institute for Materials Science (NIMS), 1-2-1 Sengen, Tsukuba, Ibaraki 305-0047, Japan*
[2]*Department of Physics, Sophia University, 7-1 Kioi-cho, Chiyoda-ku, Tokyo 102-8554, Japan*
[3]*Laboratory for Neutron Scattering and Imaging, Paul Scherrer Institut (PSI), CH-5232 Villigen PSI, Switzerland*
(Dated: June 30, 2015)

We investigated the crystal and magnetic structures of the spin-1/2 frustrated antiferromagnet $Cu_3Mo_2O_9$ in which the spin system consists of antiferromagnetic chains and dimers. The space group at room temperature has been reported to be orthorhombic *Pnma* (No. 62). We infer that the space group above $T_N = 7.9$ K is monoclinic $P2_1/m$ (No. 11) from the observation of reflections forbidden in *Pnma* in x-ray powder diffraction experiments at room temperature. We determined the magnetic structure of $Cu_3Mo_2O_9$ in neutron powder diffraction experiments. Magnetic moments on dimer sites lie in the *ac* planes. The magnitudes are $0.50 \sim 0.74\mu_B$. Moments on chain sites may exist but the magnitudes are very small. The magnetic structure indicates that a partial disordered state is realized. We consider the origin of the magnetic structure, weak ferromagnetism, and electric polarization.

PACS numbers: 75.10.Jm, 75.10.Pq, 75.25.-j, 75.47.Lx

I. INTRODUCTION

Several frustrated antiferromagnets exhibit intriguing magnetic states such as the quantum spin-liquid state [1], the chiral ordered state [2, 3], the spin nematic or the multipolar state [4, 5], and the spin-gel state [6]. Among frustrated antiferromagnets, frustrated spin chains provide grounds for studies of exotic quantum phases caused by combination of frustration and quantum fluctuation. In the Heisenberg spin-1/2 chain with antiferromagnetic (AF) nearest-neighbor (NN) and next-nearest-neighbor (NNN) exchange interactions (J_{NN} and J_{NNN} interactions, respectively), the ground state(s) are a gapless spin-singlet state designated as Tomonaga-Luttinger liquid and two-folded-degenerated gapped spin-singlet states for $0 \leq J_{NNN} < 0.241J_{NN}$ and $0.241J_{NN} < J_{NNN}$, respectively [7–9]. In the spin-Peierls substance $CuGeO_3$ [10–12], both the interactions are considered to exist [13–15]. It is inferred that a large spin gap observed in Raman scattering experiments of 3.5 % Mg-doped $CuGeO_3$ under high pressures is generated not only by the spin-Peierls transition but also by the frustration between the two interactions [16]. In the spin-1/2 chain with ferromagnetic J_{NN} and AF J_{NNN} interactions in the presence of magnetic fields, theoretical studies predict various quantum phases including the vector chiral phase, the spin nematic phase, phases with multipole order, and the spin-density-wave phases [17–26]. Several model substances have been found and are summarized in Table 1 in Ref. [27] or Fig. 5 in Ref. [28]. Experimental results are compared with theoretical results [22, 26]. In the frustrated diamond-chain system, three ground states appear according to relative intensities among exchange interactions [29]. A spin-liquid ground state and a 1/3 magnetization plateau were found in the model compound $Cu_3(CO_3)_2(OH)_2$ [30].

$Cu_3Mo_2O_9$ provides a different frustrated spin-1/2 AF chain [31]. Figure 1 shows schematically the spin system in $Cu_3Mo_2O_9$. Here, we assume that the space group SG is orthorhombic *Pnma* (No. 62) [32, 33]. There are three crystallographic Cu^{2+} sites having spin-1/2. Four types of NN exchange interactions between Cu spins exist. The J_4 interaction forms AF chains parallel to the *b* axis of Cu1 spins. The J_3 interaction forms AF dimers in *ac* planes of Cu2 and Cu3 spins. The J_1 and J_2 interactions connect chains and dimers. The four NN interactions form distorted tetrahedral spin chains. Magnetic frustration exists in each distorted tetrahedral spin chain. We also consider interchain interactions (J_{ac} and J_a interactions) shown in Fig. 1(b). As will be described later, we infer that the space group above the transition temperature $T_N = 7.9$ K is monoclinic $P2_1/m$ (No. 11), although deviations from the average symmetry (*Pnma*) are very small. In the crystal structure with $P2_1/m$, corner (α) and center (β) distorted tetrahedral spin chains are inequivalent.

We determined dispersion relations of magnetic excitations from inelastic neutron scattering results [34] of a single crystal synthesized using the continuous solid-state crystallization method [35]. We observed hybridization of magnetic excitations of the chains and dimers. The dispersion relations can be explained using the above spin model with $J_4 = 4.0$ meV, $J_3 = 5.8$ meV, $J_1 \sim 1$ meV, $J_2 \sim 1$ meV, $J_{ac} = 0.19$ meV (AF), and $J_a = -0.19$ meV (ferromagnetic) based on a chain mean-field theory with random phase approximation [34, 36–38] or with

*Electronic address: HASE.Masashi@nims.go.jp

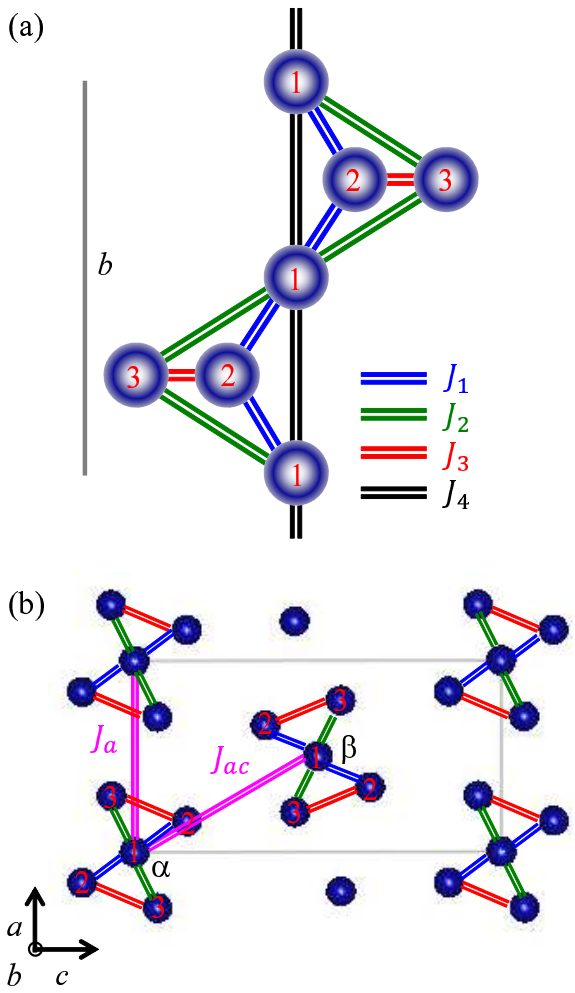

FIG. 1: (Color online) The spin system in $Cu_3Mo_2O_9$. Here, we assume that the space group is orthorhombic $Pnma$ (No. 62) [32, 33]. There are three crystallographic Cu^{2+} sites having spin-1/2. Gray lines correspond to lattice constants. (a) A distorted tetrahedral spin chain parallel to the b axis formed by the four types of nearest-neighbor exchange interactions. The J_4 interaction forms AF chains of Cu1 spins. The J_3 interaction forms AF dimers of Cu2 and Cu3 spins. The J_1 and J_2 interactions connect the chains and dimers. (b) Corner (α) and center (β) distorted tetrahedral spin chains projected on the ac plane. To explain dispersion relations of magnetic excitations, we consider J_{ac} and J_a interchain interactions in addition to $J_1 \sim J_4$ interactions. We infer that the space group above $T_N = 7.9$ K is monoclinic $P2_1/m$ (No. 11), although deviations from the average symmetry ($Pnma$) are very small. The a, b, and c axes in $Pnma$ correspond to the a, b, and c axes in $P2_1/m$, respectively. In the crystal structure with $P2_1/m$, α and β distorted tetrahedral spin chains are inequivalent.

$J_4 = 6.50$ meV, $J_3 = 5.70$ meV, $|J_1 - J_2| = 3.06$ meV, $J_{ac} = 0.04$ meV, and $J_a = -0.04$ meV based on a spin-wave theory [39].

$Cu_3Mo_2O_9$ exhibits both AF long-range order and electric polarization below $T_N = 7.9$ K, meaning that $Cu_3Mo_2O_9$ is a multiferroic substance [40]. Weak ferromagnetism appears only in finite magnetic fields parallel to the a or c axis [31]. The weak ferromagnetism disappears by slight substitution of Zn (0.5 %) for Cu sites [41]. The electric polarization appears parallel to the c axis at zero magnetic field and becomes parallel to the a axis in the magnetic field parallel to the c axis with $H > 8$ T. Several magnetic-field induced phase transitions and 2/3 magnetization plateau appear in the magnetization curves up to 74 T [42, 43]. The magnetic and dielectric properties change simultaneously at the transition fields. Temperature - magnetic field phase diagrams have been obtained [43]. Raman scattering experiments were performed [44]. The Raman scattering spectra did not change at T_N. Therefore, change of the crystal structure caused by the multiferroic transition is negligibly small.

It is important to determine the magnetic structure of $Cu_3Mo_2O_9$ to understand the above-mentioned results. Another group performed neutron powder diffraction experiments and reported the magnetic structure of $Cu_3Mo_2O_9$ [45]. Ferromagnetic behavior parallel to the b axis is expected in the result, whereas the ferromagnetic behavior parallel to the a or c axis was observed in our magnetization results of single crystals [31]. We considered that reinvestigation of the magnetic structure is necessary. Accordingly, we performed neutron powder diffraction experiments.

II. EXPERIMENTAL METHODS

We synthesized $Cu_3Mo_2O_9$ powder using a solid-state-reaction method at 1023 K in air for 150 h with intermediate grindings. We performed X-ray powder diffraction experiments at room temperature using a RIGAKU RINT-TTR III diffractometer. The wavelength λ is 1.542 Å ($Cu\ K_\alpha$). We carried out neutron powder diffraction experiments at the Swiss spallation neutron source (SINQ) at Paul Scherrer Institute (PSI). We used the high-resolution powder diffractometer for thermal neutrons (HRPT) in the high intensity mode ($\Delta d/d \geq 1.8 \times 10^{-3}$) [46] and the high-intensity cold neutron powder diffractometer (DMC). We used neutrons with $\lambda = 1.886$ and 4.507 Å at HRPT and DMC diffractometers, respectively. Powder was filled into a vanadium container with 8 mm diameter and 55 mm height for the HRPT experiments and that with 10 mm diameter and 55 mm height for the DMC experiments.

We performed Rietveld refinements of the crystal and magnetic structures using the `FULLPROF Suite` program package [47] with its internal tables for scattering lengths and magnetic form factors. Symmetry analysis was done by using `ISODISTORT` tool based on `ISOTROPY` software

[48, 49] and BASIREP program of FULLPROF Suite.

III. RESULTS AND ANALYSES

A. Reinvestigation into the crystal structure above T_N

The space group of $Cu_3Mo_2O_9$ at room temperature has been reported to be orthorhombic *Pnma* (No. 62) [32, 33]. As will shown later, the symmetry of the crystal structure is important to consider weak ferromagnetism and electric polarization. Therefore, we reinvestigated the crystal structure above T_N. We measured high statistics x-ray powder diffraction patterns at 290 K to investigate whether reflections forbidden in *Pnma* were present or not. As shown in Fig. 2, we found five weak reflections that were forbidden in *Pnma*. We estimated the d values of the five reflections as 14.8(2), 7.59(2), 5.14(3), 5.02(2), and 2.936(3) Å from lower to higher 2θ. Assuming an orthorhombic crystal structure, we calculated the lattice constants as $a = 7.685(2), b = 6.878(1)$, and $c = 14.650(3)$ Å from an x-ray diffraction pattern at 290 K between $2\theta = 5$ and 80°. We obtained the d values as 14.650(3), 7.685(2), 5.125(2), 5.014(2), and 2.930(1) Å for forbidden reflections at (001), (100), (110), (012), and (005). We consider that we can assign the indices to the five reflections. The diffraction results suggest that the space group at 290 K could have a lower symmetry than *Pnma*. In maximal subgroups of *Pnma*, only monoclinic $P2_1/m$ (No. 11) can have all the forbidden reflections. The a, b, and c axes in *Pnma* correspond to the a, b, and c axes in $P2_1/m$, respectively. We observed no phase transition above T_N in the specific heat of $Cu_3Mo_2O_9$ [31]. Consequently, we tentatively suggest that the space group above T_N is $P2_1/m$. The five reflections forbidden in *Pnma* are very weak. For example, the forbidden (005) reflection is weaker than the weak allowed (122) reflection shown in Fig. 2(d), which is only 0.72 % of the largest Bragg reflection at (020). Accordingly, deviations from the average symmetry are very small and we cannot rigorously prove that the space group at 290 K is $P2_1/m$.

The circles in Fig. 3 show a neutron powder diffraction pattern of $Cu_3Mo_2O_9$ at 12 K just above T_N = 7.9 K recorded using the HRPT diffractometer with $\lambda = 1.886$ Å. We performed Rietveld refinements using *Pnma* to evaluate crystal structure parameters at 12 K. The line on the experimental pattern indicates the result of Rietveld refinements. The line agrees well with the experimental pattern. The refined crystal structure parameters are presented in Table I. We performed symmetry analysis and Rietveld refinements based on both $P2_1/m$ and *Pnma* to determine the magnetic structure. We expected that atomic positions determined using $P2_1/m$ would be almost the same as those determined using *Pnma* because the forbidden reflections are very weak. Therefore, we used the values in Table I for the following Rietveld refinements to determine the magnetic structure. We describe below the relation between the positions in *Pnma* and $P2_1/m$. The basis transformation is given by identity matrix without origin shift. The Cu1 ($4a$) position in *Pnma* is split into Cu11 ($2a$) and Cu12 ($2d$) positions in $P2_1/m$. The Cu2 and Cu3 ($4c$) positions are split into Cu21 and Cu22 ($2e$)-, and Cu31 and Cu32 ($2e$)-positions, respectively. In $P2_1/m$, the corner (α) and center (β) distorted tetrahedral spin chains are inequivalent.

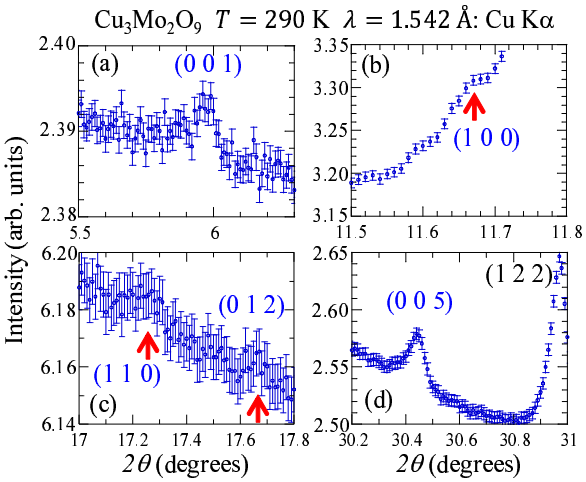

FIG. 2: (Color online) X-ray powder diffraction patterns of $Cu_3Mo_2O_9$ at 290 K measured using a RIGAKU RINT-TTR III diffractometer ($\lambda = 1.542$ Å, Cu K_α). Five reflections forbidden in *Pnma* were observed at (001), (100), (110), (012), and (005).

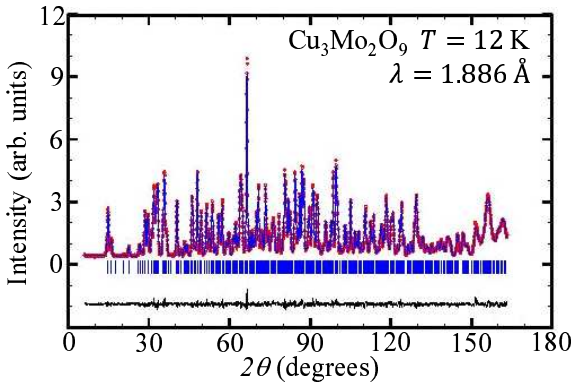

FIG. 3: (Color online) A neutron powder diffraction pattern of $Cu_3Mo_2O_9$ at 12 K (above the transition temperature T_N = 7.9 K) measured using the HRPT diffractometer ($\lambda = 1.886$ Å). Lines on the observed pattern and at the bottom show a Rietveld refined pattern obtained using the crystal structure with *Pnma* (No. 62) and the difference between the observed and the Rietveld refined patterns, respectively. Hash marks represent positions of nuclear reflections.

TABLE I: Structural parameters of $Cu_3Mo_2O_9$ derived from Rietveld refinements of the HRPT neutron powder diffraction pattern at 12 K. We used orthorhombic $Pnma$ (No. 62). The lattice constants at 12 K are $a = 7.629(1)$ Å, $b = 6.876(1)$ Å, and $c = 14.573(1)$ Å. Estimated standard deviations are shown in parentheses. The reliability factors of the refinement are $R_p = 3.26$ %, $R_{wp} = 4.16$ %, $R_{exp} = 2.75$ %, and $\chi^2 = 2.29$.

Atom	Site	x	y	z	B_{iso} Å^2
Cu1	4a	0	0	0	0.23(3)
Cu2	4c	0.1620(2)	0.75	0.1430(1)	0.09(3)
Cu3	4c	0.2064(2)	0.25	0.4373(1)	0.14(3)
Mo1	4c	0.2657(3)	0.25	0.1696(1)	0.18(3)
Mo2	4c	0.1547(3)	0.75	0.3885(1)	0.19(4)
O1	4c	0.0875(3)	0.75	0.0159(1)	0.22(5)
O2	4c	0.2075(3)	0.75	0.2715(2)	0.32(4)
O3	4c	0.4310(3)	0.75	0.0969(2)	0.27(5)
O4	8d	0.2481(2)	0.9636(2)	0.4397(1)	0.31(3)
O5	8d	0.1410(2)	0.0369(2)	0.1373(1)	0.42(3)
O6	4c	0.3029(3)	0.25	0.2857(2)	0.44(4)
O7	4c	0.4692(3)	0.25	0.1103(2)	0.33(5)

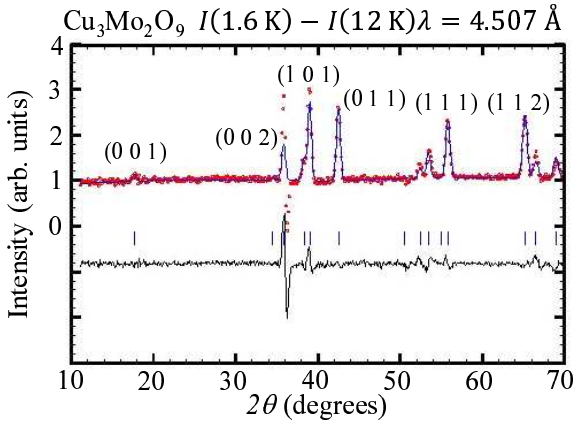

FIG. 4: (Color online) A difference pattern made by subtracting a neutron powder diffraction pattern of $Cu_3Mo_2O_9$ at 12 K from that at 1.6 K ($T_N = 7.9$ K). The diffraction patterns were measured using the DMC diffractometer ($\lambda = 4.507$ Å). Lines on the observed pattern show a Rietveld refined pattern obtained using Γ_1^- ($\tau 2$) in $P2_1/m$. Lines at the bottom show the difference between the observed and the Rietveld refined patterns. Hash marks represent positions of magnetic reflections. We described indices of several magnetic reflections.

B. Magnetic structure

We measured neutron powder diffraction patterns at 1.6 and 12 K (below and above $T_N = 7.9$ K, respectively) using the DMC diffractometer with $\lambda = 4.507$ Å. Figure 4 shows the difference pattern made by subtracting the 12 K diffraction pattern from the 1.6 K one. Several magnetic reflections are apparent at 1.6 K. All the reflections can be indexed in the chemical cell with the propagation vector $\mathbf{k} = \mathbf{0}$.

The magnetic reflections are much weaker than major nuclear reflections. Therefore, we have performed the analysis for the difference pattern shown in Fig. 4 to determine the magnetic structure of $Cu_3Mo_2O_9$. For $\mathbf{k} = \mathbf{0}$, there are four one dimensional (1D) real irreducible representations (IRs) that enter the magnetic representation decomposition, resulting in four possible Shubnikov groups based on $P2_1/m$. The best-fit candidate is $P2_1/m'$, which corresponds to Γ_1^- ($\tau 2$). The nomenclature for the IR is given according to Ref. [49] with Kovalev's notation in the parenthesis. The a and c components of magnetic moments are allowed on the dimer sites (2e), whereas the magnetic moments on the chain sites (2a and 2d) are zero by symmetry of Γ_1^-. There are two IRs even by inversion operator Γ_2^+ ($\tau 3$) and Γ_1^+ ($\tau 1$), that allow non-zero chain moments. We performed Rietveld refinements using Γ_1^- for dimer moments and Γ_2^+ or Γ_1^+ for chain moments. In both cases, the reliability factors are smallest for the chain moments close to zero.

As shown in Fig. 4, the experimental pattern can be explained well by the line calculated using only $P2_1/m'$. The reliability factors are $R_{wp} = 4.90$ %, $R_{exp} = 2.85$ %, and $\chi^2 = 2.95$. The magnetic structure is shown in Fig. 5. Magnetic moments on dimer sites are $\mathbf{M}_{21} = (0.57(2), 0, 0.04(3))\mu_B$ on Cu21 sites, $\mathbf{M}_{22} = (0.46(3), 0, -0.50(3))\mu_B$ on Cu22 sites, $\mathbf{M}_{31} = (0.27(4), 0, 0.69(3))\mu_B$ on Cu31 sites, and $\mathbf{M}_{32} = (0.04(4), 0, -0.50(3))\mu_B$ on Cu32 sites. The magnitude of the moments is $M_{21} = 0.57(2)\mu_B$, $M_{22} = 0.69(3)\mu_B$, $M_{31} = 0.74(4)\mu_B$, and $M_{32} = 0.50(3)\mu_B$. The angle between two moments in Cu21-Cu32 and Cu22-Cu31 dimers are 90(8)° and 116(6)°, respectively. Two neighboring dimer moments in each distorted tetrahedral spin chain are antiparallel to each other as indicated by the blue or green line. The chain moments may exist but the magnitudes are very small, meaning that spins in chains are nearly disordered. The magnetic structure indicates that a partial disordered (PD) state is realized. In the previous papers [31, 41], we inferred that the main component of ordered moments in chains was the b component and that spins in dimers were nearly spin singlet.

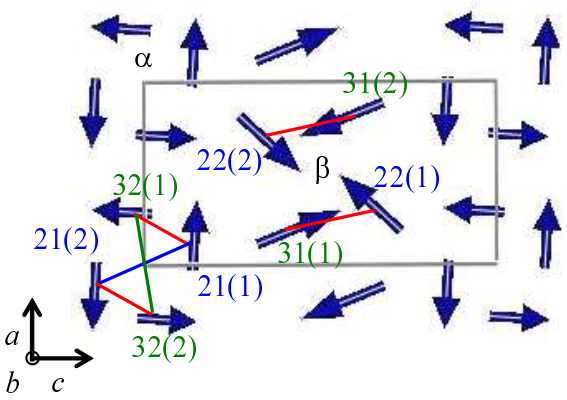

FIG. 5: (Color online) The magnetic structure of $Cu_3Mo_2O_9$ obtained using Γ_1^- ($\tau 2$) in $P2_1/m$. Magnetic moment vectors in dimers are $\mathbf{M}_{21} = (0.57(2), 0, 0.04(3))\mu_B$ on Cu21(1) sites, $\mathbf{M}_{22} = (0.46(3), 0, -0.50(3))\mu_B$ on Cu22(1) sites, $\mathbf{M}_{31} = (0.27(4), 0, 0.69(3))\mu_B$ on Cu31(1) sites, and $\mathbf{M}_{32} = (0.04(4), 0, -0.50(3))\mu_B$ on Cu32(1) sites. Symmetry operators of moments on 2*e* sites (dimer moments) for Γ_1^- ($\tau 2$) are (1) $[u, 0, w]$ and (2) $[\bar{u}, 0, \bar{w}]$. The chain moments are very small if they exist.

The previous inferences are incorrect.

We investigated the magnetic structure assuming *Pnma* that has been reported as the space group at room temperature. As described below, the obtained magnetic structures are similar to that in Fig. 5. In the case of $\mathbf{k} = \mathbf{0}$, there are eight 1D real IRs, resulting in eight Shubnikov groups based on *Pnma*. The best-fit candidate is $Pnm'a$, which corresponds to Γ_4^- ($\tau 4$). The *a* and *c* components of ordered magnetic moments can be finite on dimer sites (4*c*), whereas no ordered magnetic moment on chain sites (4*a*) is allowed by symmetry of Γ_4^-. In addition, the (001) magnetic reflection observed at $2\theta = 17.7°$ is forbidden in Γ_4^-. There are four IRs even by inversion operator that enter the magnetic representation decomposition for the chain moments. Among the four, the (001) magnetic reflection is allowed in Γ_2^+ ($\tau 7$) and Γ_1^+ ($\tau 1$). In refinements using Γ_4^- and Γ_2^+ for dimer and chain moments, respectively, we obtained magnetic moments as $\mathbf{M}_1 = (0.085(9), 0, 0)\mu_B$ on Cu1 sites, $\mathbf{M}_2 = (0.555(8), 0, 0.283(6))\mu_B$ on Cu2 sites, and $\mathbf{M}_3 = (0.132(7), 0, 0.604(6))\mu_B$ on Cu3 sites. The reliability factors are $R_{wp} = 5.02$ %, $R_{exp} = 2.86$ %, and $\chi^2 = 3.08$. The magnitude of the Cu2 and Cu3 moments is $0.62(1)\mu_B$. The angle between two moments in each dimer is 105(2)°. In refinements using Γ_4^- and Γ_1^+ for dimer and chain moments, respectively, we obtained magnetic moments as $\mathbf{M}_1 = (0, 0.085(9), 0.13(2))\mu_B$ on Cu1 sites $\mathbf{M}_2 = (0.543(9), 0, 0.289(7))\mu_B$ on Cu2 sites, and $\mathbf{M}_3 = (0.141(7), 0, 0.593(8))\mu_B$ on Cu3 sites. The reliability factors are $R_{wp} = 4.97$ %, $R_{exp} = 2.86$ %, and $\chi^2 = 3.02$. The magnitude of the Cu1, Cu2, and Cu3 moments is 0.16(2), 0.62(1), and $0.61(1)\mu_B$, respectively. The angle between two moments in each dimer is 105(2)°.

IV. DISCUSSION

A. the origin of the magnetic structure

We consider the origin of the magnetic structure in $Cu_3Mo_2O_9$. To avoid complicated explanations, we use Cu1, Cu2, and Cu3 to indicate Cu sites. As described, the four types of NN interactions ($J_1 \sim J_4$ interactions) shown in Fig. 1 generate magnetic frustration. Six NN interactions influence each Cu1 spin, whereas only three NN interactions influence each Cu2 or Cu3 spin. Probably, the frustration is more effective for Cu1 spins than Cu2 and Cu3 spins. Therefore, Cu1 spins are nearly disordered, whereas Cu2 and Cu3 spins can be ordered. Two neighboring Cu2 (Cu3) moments in each distorted tetrahedral spin chain are antiparallel to each other as indicated by the blue (green) line in Fig. 5. The internal magnetic fields generated by Cu2 or Cu3 ordered moments are canceled out on Cu1 sites in the magnetic structure. Therefore, classical magnetic energy is independent of the direction of Cu1 moments in the absence of magnetic anisotropy. The magnetic structure of the Cu2 and Cu3 moments allow the nearly disordered state of Cu1 spins.

A similar PD state is seen in the frustrated three-leg-ladder Heisenberg antiferromagnets $Cu_3(OH)_4AO_4$ (A = S or Se) [50, 51]. Cu moments within the inner leg remain random, whereas Cu moments within the two outer legs are ordered. Six NN interactions influence each inner Cu spin, whereas four NN interactions influence each outer Cu spin. The frustration may be more effective for inner Cu spins than outer Cu spins as expected in $Cu_3Mo_2O_9$. In addition to $Cu_3(OH)_4AO_4$ (A = S or Se), a part of spins are perfectly or nearly disordered in the ordered state in several frustrated Heisenberg antiferromagnets such as the spinel antiferromagnet $GeNi_2O_4$ [52], the pyrochlore antiferromagnet $Gd_2Ti_2O_7$, [53] and the triangular lattice antiferromagnets $CuFeO_2$ [54] and Ag_2CrO_2 [55]. Exchange interactions in long $M - M$ bonds, where M represents a magnetic ion, play an important role in the occurrence of the PD states.

Table II shows possible Shubnikov magnetic groups appearing as a result of mixing of two IRs. Among them, bond alternation of the J_4 interaction is possible in *Pm* (No. 6) and $Pmc2_1$ (No. 26). The bond alternation of the J_4 interaction may be the origin of the very small Cu1 moment. Bond alternation of NN interactions generates a gapped spin-singlet ground state in an AF spin chain as in the spin-Peierls system. The values of S^T and S_z^T are 0 in a spin-singlet ground state. Here, S^T and S_z^T represent a value and a z value, respectively, of the sum of spin operators. Other $S_z^T = 0$ states can be hybridized with the spin-singlet ground state of an AF alternating spin chain by other interactions [56]. States with $S^T > 0$ and $S_z^T = 0$ are magnetic. For example, $S_z^T = 0$ is zero

in a collinear two-sublattice AF ordered state, although the state is not an eigenstate of the AF Heisenberg models. As a result, the ground state of the AF alternating spin chain can be magnetic by the hybridization of plural $S_z^{\rm T} = 0$ states. When AF long-range order occurs, the magnitude of the ordered moments is expected to be larger for a smaller spin gap. The alternation ratio is probably very close to 1 and a spin gap is very small. The spin gap of Cu1 spins is less than 0.2 meV in inelastic neutron scattering results of $Cu_3Mo_2O_9$. Accordingly, the bond alternation of the J_4 interaction is not the origin of the very small Cu1 moment.

The moments in AF dimers are reduced from a classical value ($\sim 1\mu_{\rm B}$). Probably, the magnetic frustration generates the reduction of the moments. In addition, character of a spin-singlet pair may be overlapped and may cause the reduction of the moments [57]. We do not understand the reason that the angle between two moments in AF dimers (90(8)° or 116(6)°) is different from 180° (antiparallel configuration). As described, long-distance interactions exist in several frustrated Heisenberg antiferromagnets showing a PD state. Long-distance interactions may exist in $Cu_3Mo_2O_9$ and may affect determination of the angle between two moments in AF dimers. The 2/3 magnetization plateau appears in the magnetization curves of $Cu_3Mo_2O_9$ [43]. In a Heisenberg model with bilinear and biquadratic terms [$\mathbf{S}_i \cdot \mathbf{S}_j$ and $(\mathbf{S}_i \cdot \mathbf{S}_j)^2$ terms, respectively], magnetization plateau can appear as in $CdCr_2O_4$ [58]. We are seeking for a model that can explain the magnetic excitations, the magnetization curves, and the magnetic structure.

B. consideration to other experimental results

We comment on the signs of the exchange interactions between spins on chain sites. From the dispersion relations of the magnetic excitations, the J_4 interaction forming Cu1 spin chains parallel to the b axis and the interchain J_{ac} interaction are antiferromagnetic, whereas the interchain J_a interaction is ferromagnetic [34, 39]. The signs of the interactions agree with the signs of the b components on $2a$ and $2d$ sites for Γ_2^+ in $P2_1/m$ and the signs of the a and c components on $2a$ and $2d$ sites for Γ_1^+ in $P2_1/m$, although the chain moments are nearly disordered. Spin chains can show dispersive magnetic excitations even in the absence of magnetic long-range order. The disordered component generates the magnetic excitations of the chains.

We consider the weak ferromagnetism in magnetic fields parallel to the a or c axis [31] and the electric polarization parallel to the c axis at zero magnetic field [40] below $T_{\rm N} = 7.9$ K in $Cu_3Mo_2O_9$. As described in Table II, if the IR for the chain moments is Γ_2^+ in $P2_1/m$, the Shubnikov group for the magnetic structure is Pm' from the mixing of Γ_1^- and Γ_2^+. Dimer sites are $1a$ or $1b$ sites. Therefore, all the dimer sites are independent. Symmetry operators of chain moments on $2a$ and $2d$ sites are (1) $[u, v, w]$ and (2) $[u, \bar{v}, w]$. The weak ferromagnetism perpendicular to the b axis is possible in Pm'. The electric polarization perpendicular to the b axis is possible in the crystal structure with the space group Pm. Considering the basis transformation, the b axis in Pm corresponds to the b axis in $P2_1/m$. Consequently, the experimental results of the weak ferromagnetism and electric polarization may be explained by the Pm' model described in the first line in Table II. The other models in Table II, on the other hand, cannot explain the experimental results.

We consider that the origin of the weak ferromagnetism is the dimer moments because of the following reasons. The chain moments are very small if they exist. It may be doubtful that the chain moments can have the observable weak ferromagnetism. The weak ferromagnetism disappears by substitution of Zn for Cu sites [41]. We performed neutron powder diffraction experiments on $Cu_{2.88}Zn_{0.12}Mo_2O_9$ and $Cu_{2.85}Zn_{0.15}Mo_2O_9$ using the HRPT diffractometer. We observed a few magnetic reflections. Probably, the propagation vector is $\mathbf{k} = \mathbf{0}$ as in $Cu_3Mo_2O_9$. We evaluated crystal structure parameters above $T_{\rm N}$ assuming $Pnma$. Most of Zn ions enter Cu3 sites, the remaining Zn ions enter Cu2 sites, and almost no Zn ions enter Cu1 sites. Influence of Zn substitution is more effective for Cu2 and Cu3 sites than for Cu1 sites. The results suggest that Cu2 and Cu3 moments (dimer moments) are responsible for the weak ferromagnetism. We will determine the magnetic structure of $Cu_{3-x}Zn_xMo_2O_9$ to investigate the origin of the weak ferromagnetism and the reason that the weak ferromagnetism disappears by substitution of Zn for Cu sites.

V. CONCLUSION

We investigated the crystal and magnetic structures of the spin-1/2 frustrated antiferromagnet $Cu_3Mo_2O_9$ in which the spin system consists of antiferromagnetic chains and dimers. The space group at room temperature has been reported to be orthorhombic $Pnma$ (No. 62). We observed reflections forbidden in $Pnma$ in x-ray powder diffraction experiments at room temperature. We infer that the space group above $T_{\rm N} = 7.9$ K is monoclinic $P2_1/m$ (No. 11) that is one of maximal subgroups of $Pnma$. We determined the magnetic structure of $Cu_3Mo_2O_9$ in neutron powder diffraction experiments. The experimental diffraction pattern can be explained well by the line calculated using the irreducible representation (IR) Γ_1^- ($\tau 2$) in $P2_1/m$. Magnetic moments on dimer sites lie in the ac planes. The magnitudes are $0.50 \sim 0.74\mu_{\rm B}$. The angle between two moments in dimers is 90(8)° or 116(6)°. The moments on chain sites may exist but the magnitudes are very small. The magnetic structure indicates that a partial disordered state is realized. Probably, magnetic frustration influences the magnetic structure. If the IR for the chain moments is Γ_2^+ ($\tau 3$) in $P2_1/m$, the Shubnikov group for the magnetic structure is Pm' from the mixing of Γ_1^- and Γ_2^+.

TABLE II: Possible ferromagnetic moment (FM) and electric polarization (EP) in the Shubnikov groups obtained by mixing of two IRs of the parent space groups. The columns indicate A: the parent space group to be considered initially, B: the two mixed IRs, C: the Shubnikov group obtained by the mixing with the number in BNS settings [49], and D and E: the direction of the possible FM and EP, respectively, in the basis of the parent space group of the column A (the Shubnikov group of the column C). The symbol "-" means no FM or EP. The third and sixth lines are added to indicate that FM and EP are impossible in Shubnikov group based on single IR.

A	B	C	D: FM	E: EP
$P2_1/m$	Γ_1^-, Γ_2^+	Pm' (6.20)	$\perp b$ ($\perp b$)	$\perp b$ ($\perp b$)
	Γ_1^-, Γ_1^+	$P2_1$ (4.7)	$\parallel b$ ($\parallel b$)	$\parallel b$ ($\parallel b$)
	Γ_1^-	$P2_1/m'$ (11.53)	- (-)	- (-)
$Pnma$	Γ_4^-, Γ_2^+	$Pm'c2_1'$ (26.68)	$\parallel c$ ($\parallel b$)	$\parallel a$ ($\parallel c$)
	Γ_4^-, Γ_1^+	$Pna2_1$ (33.144)	- (-)	$\parallel b$ ($\parallel c$)
	Γ_4^-	$Pnm'a$ (62.444)	- (-)	- (-)

The weak ferromagnetism perpendicular to the b axis is possible in Pm'. The electric polarization perpendicular to the b axis is possible in the crystal structure with the space group Pm (No. 6). The b axis in Pm corresponds to the b axis in $P2_1/m$ and $Pnma$. Consequently, the experimental results of the weak ferromagnetism and electric polarization may be explained by the Pm' model.

Acknowledgments

We are grateful to H. Eisaki, T. Goto, T. Ito, K. Kaneko, Y. Kawamura, R. Kiyanagi, M. Kohno, T. Masuda, M. Matsuda, M. Matsumoto, S. Matsumoto, Y. Noda, K. Oka, T. Suzuki, K. Tomiyasu, and O. Zaharko for fruitful discussion or experimental supports. The neutron powder diffraction experiments were performed by using the DMC and HRPT diffractometers at SINQ, PSI, Switzerland (proposal nos. 20131441 and 20131464, respectively). The experiments were transferred from 5G:PONTA at JRR-3 with the approval of Institute for Solid State Physics, The University of Tokyo (proposal nos. 14806 and 14807) and Japan Atomic Energy Agency, Tokai, Japan. This work was partially supported by grants from NIMS.

[1] P. W. Anderson, Mater. Res. Bull. **8**, 153 (1973).
[2] S. Miyashita and H. Shiba, J. Phys. Soc. Jpn. **53**, 1145 (1984).
[3] S. Onoda and N. Nagaosa, Phys. Rev. Lett. **99**, 027206 (2007).
[4] H. Tsunetsugu and M. Arikawa, J. Phys. Soc. Jpn. **75**, 083701 (2006).
[5] M. E. Zhitomirsky, Phys. Rev. B **78**, 094423 (2008).
[6] H. Kawamura, A. Yamamoto, and T. Okubo, J. Phys. Soc. Jpn. **79**, 023701 (2010).
[7] F. D. M. Haldane, Phys. Rev. B **25**, 4925 (1982).
[8] F. D. M. Haldane, Phys. Rev. B **26**, 5257 (1982).
[9] K. Okamoto and K. Nomura, Phys. Lett. A **169**, 433 (1992).
[10] M. Hase, I. Terasaki, and K. Uchinokura, Phys. Rev. Lett. **70**, 3651 (1993).
[11] M. Hase, I. Terasaki, Y. Sasago, K. Uchinokura, and H. Obara, Phys. Rev. Lett. **71**, 4059 (1993).
[12] M. Hase, I. Terasaki, K. Uchinokura, M. Tokunaga, N. Miura, and H. Obara, Phys. Rev. B **48**, 9616 (1993).
[13] J. E. Lorenzo, K. Hirota, G. Shirane, J. M. Tranquada, M. Hase, K. Uchinokura, H. Kojima, I. Tanaka, and Y. Shibuya, Phys. Rev. B **50**, 1278 (1994).
[14] G. Castilla, S. Chakravarty, and V. J. Emery, Phys. Rev. Lett. **75**, 1823 (1995).
[15] J. Riera and A. Dobry, Phys. Rev. B **51**, 16098 (1995).
[16] Y. Tanokura, Y. Oono, S. Ikeda, H. Kuroe, T. Sekine, T. Masuda and K. Uchinokura, Phys. Rev. B **68**, 054412 (2003).
[17] A. V. Chubukov, Phys. Rev. B **44**, 4693 (1991).
[18] A. Kolezhuk and T. Vekua, Phys. Rev. B **72**, 094424 (2005).
[19] F. Heidrich-Meisner, A. Honecker, and T. Vekua, Phys. Rev. B **74**, 020403(R) (2006).
[20] T. Vekua, A. Honecker, H.-J. Mikeska, and F. Heidrich-Meisner, Phys. Rev. B **76**, 174420 (2007).
[21] L. Kecke, T. Momoi, and A. Furusaki, Phys. Rev. B **76**, 060407(R) (2007).
[22] T. Hikihara, L. Kecke, T. Momoi, and A. Furusaki, Phys. Rev. B **78**, 144404 (2008).
[23] J. Sudan, A. Luscher, and A. M. Läuchli, Phys. Rev. **B** 80, 140402(R) (2009).
[24] M. Sato, T. Momoi, and A. Furusaki, Phys. Rev. B **79**, 060406(R) (2009).
[25] F. Heidrich-Meisner, I. P. McCulloch, and A. K. Kolezhuk, Phys. Rev. B **80**, 144417 (2009).
[26] M. Sato, T. Hikihara, and T. Momoi, Phys. Rev. B **83**, 064405 (2011).
[27] M. Hase, H. Kuroe, K. Ozawa, O. Suzuki, H. Kitazawa, G. Kido, and T. Sekine, Phys. Rev. B **70**, 104426 (2004).
[28] S.-L. Drechsler, O. Volkova, A. N. Vasiliev, N. Tristan, J. Richter, M. Schmitt, H. Rosner, J. Málek, R. Klingeler, A. A. Zvyagin, and B. Büchner, Phys. Rev. Lett. **98**, 077202 (2007).
[29] K. Okamoto, T. Tonegawa, Y. Takahashi and M. Kaburagi, J. Phys. Condens. Matter **15**, 5979 (1999).

[30] H. Kikuchi, Y. Fujii, M. Chiba, S. Mitsudo, T. Idehara, T. Tonegawa, K. Okamoto, T. Sakai, T. Kuwai and H. Ohta, Phys. Rev. Lett. **94**, 227201 (2005).

[31] T. Hamasaki, T. Ide, H. Kuroe, T. Sekine, M. Hase, I. Tsukada, and T. Sakakibara, Phys. Rev B **77**, 134419 (2008).

[32] U. Steiner and W. Reichelt: Acta Cryst. C **53**, 1371 (1997).

[33] W. Reichelt, U. Steiner, T. Söhnel, O. Oeckler, V. Duppel and L. Kienle, Z. Anorg. Allg. Chem. **631**, 596 (2005).

[34] H. Kuroe, T. Hamasaki, T. Sekine, M. Hase, K. Oka, T. Ito, H. Eisaki, K. Kaneko, N. Metoki, M. Matsuda, and K. Kakurai, Phys. Rev. B **83**, 184423 (2011).

[35] K. Oka, T. Ito, H. Eisaki, M. Hase, T. Hamasaki, H. Kuroe, and T. Sekine, J. Crystal Growth **334**, 108 (2011).

[36] F. H. L. Essler, A. M. Tsvelik, and G. Delfino, Phys. Rev. B **56**, 11001 (1997).

[37] M. Kenzelmann, A. Zheludev, S. Raymond, E. Ressouche, T. Masuda, P. Bóni, K. Kakurai, I. Tsukada, K. Uchinokura, and R. Coldea, Phys. Rev. B **64**, 054422 (2001).

[38] A. Zheludev, S. Raymond, L.-P. Regnault, F. H. L. Essler, K. Kakurai, T. Masuda, and K. Uchinokura, Phys. Rev. B **67**, 134406 (2003).

[39] M. Matsumoto, H. Kuroe, T. Sekine, and M. Hase, J. Phys. Soc. Jpn. **81**, 024711 (2012).

[40] H. Kuroe, R. Kino, T. Hosaka, M. Suzuki, S. Hachiuma, T. Sekine, M. Hase, K. Oka, T. Ito, H. Eisaki, M. Fujisawa, S. Okubo, and H. Ohta, J. Phys. Soc. Jpn. **80**, 083705 (2011).

[41] M. Hase, H. Kitazawa K. Ozawa, T. Hamasaki, H. Kuroe, and T. Sekine, J. Phys. Soc. Jpn. **77**, 034706 (2008).

[42] T. Hamasaki, H. Kuroe, T. Sekine, M. Hase, and H. Kitazawa, J. Phys.: Conf. Series **150**, 042047 (2009).

[43] H. Kuroe, K. Aoki, R. Kino, T. Sato, H. Kuwahara, T. Sekine, T. Kihara,Y. Kohama, M. Akaki, M. Tokunaga, M. Hase, T. Takehana, H. Kitazawa, K. Oka, T. Ito, and H. Eisaki, JPS Conf. Proc. **3**, 014036 (2014).

[44] T. Sato, K. Aoki, R. Kino, H. Kuroe, T. Sekine, M. Hase, K. Oka, T. Ito, and H. Eisaki, JPS Conf. Proc. **3**, 014035 (2014).

[45] S. Vilminot, G. André, and M. Kurmoo, Inorg. Chem. **48**, 2687 (2009).

[46] P. Fischer, G. Frey, M. Koch, M. Koennecke, V. Pomjakushin, J. Schefer, R. Thut, N. Schlumpf, R. Buerge, U. Greuter, S. Bondt, and E. Berruyer, Physica B, **276-278**, 146 (2000); [http://sinq.web.psi.ch/hrpt].

[47] J. Rodriguez-Carvajal, Physica B **192**, 55 (1993); [http://www.ill.eu/sites/fullprof/].

[48] H. T. Stokes and D. M. Hatch, *Isotropy Subgroups of the 230 Crystallographic Space Groups*, (World Scientific Publishing, Singapore, 1988).

[49] B. J. Campbell, H. T. Stokes, D. E. Tanner, and D. M. Hatch, J. Appl. Cryst. **39**, 607 (2006).

[50] S. Vilminot, M. Richard-Plouet, G. André, D. Swierczynski, M. Guillot, F. Bourée-Vigneron, and M. Drillon, J. Solid State Chem. **170**, 255 (2003).

[51] S. Vilminot, G. André, F. Bourée-Vigneron, M. Richard-Plouet, and M. Kurmoo, Inorg. Chem. **46**, 10079 (2007).

[52] M. Matsuda, J.-H. Chung, S. Park, T. J. Sato, K. Matsuno, H. Aruga Katori, H. Takagi, K. Kakurai, K. Kamazawa, Y. Tsunoda, I. Kagomiya, C. L. Henley, and S.-H. Lee, EPL **82**, 37006 (2008).

[53] J. R. Stewart, G. Ehlers, A. S. Wills, S. T. Bramwell, and J. S. Gardner, J. Phys.: Condens. Matter **16**, L321 (2004).

[54] M. Mekata, N. Yaguchi, T. Takagi, T. Sugino, S. Mitsuda, H. Yoshizawa, N. Hosoito, and T. Shinjo, J. Phys. Soc. Jpn. **62**, 4474 (1993).

[55] M. Matsuda, C. de la Cruz, H. Yoshida, M. Isobe, R. S. Fishman, Phys. Rev B **85**, 144407 (2012).

[56] T. Masuda, K. Kakurai, and A. Zheludev, Phys. Rev B **80**, 180412(R) (2009).

[57] K. Tomiyasu, M. K. Crawford, D. T. Adroja, P. Manuel, A. Tominaga, S. Hara, H. Sato, T. Watanabe, S. I. Ikeda, J. W. Lynn, K. Iwasa, and K. Yamada, Phys. Rev B **84**, 054405 (2011).

[58] K. Penc, N. Shannon, and H. Shiba, Phys. Rev. Lett. **93**, 197203 (2004).